Optically tunable nanoparticle contrast agents for early cancer detection: model-based analysis of gold nanoshells

Alex W. H. Lin
Nastassja A. Lewinski
Jennifer L. West
Rice University
Department of Bioengineering
PO Box 1892-MS 142
Houston, Texas 77251

Naomi J. Halas
Rice University
Department of Electrical and Computer Engineering
Houston, Texas 77251

Rebekah A. Drezek
Rice University
Department of Bioengineering
PO Box 1892-MS 142
Houston, Texas 77251
E-mail: drezek@rice.edu

Abstract. Many optical diagnostic approaches rely on changes in scattering and absorption properties to generate optical contrast between normal and diseased tissue. Recently, there has been increasing interest in using exogenous agents to enhance this intrinsic contrast with particular emphasis on the development for targeting specific molecular features of disease. Gold nanoshells are a class of core-shell nanoparticles with an extremely tunable peak optical resonance ranging from the near-UV to the mid-IR wavelengths. Using current chemistries, nanoshells of a wide variety of core and shell sizes can easily be fabricated to scatter and/or absorb light with optical cross sections often several times larger than the geometric cross section. Using gold nanoshells of different size and optical parameters, we employ Monte Carlo models to predict the effect of varying concentrations of nanoshells on tissue reflectance. The models demonstrate the importance of absorption from the nanoshells on remitted signals even when the optical extinction is dominated by scattering. Furthermore, because of the strong optical response of nanoshells, a considerable change in reflectance is observed with only a very small concentration of nanoshells. Characterizing the optical behavior of gold nanoshells in tissue will aid in developing nanoshells as contrast agents for optical diagnostics. [DOI: 10.1117/1.2141825]

Keywords: nanoshells; nanoparticles; nanotechnology; Monte Carlo; contrast agents.

Paper 05043RR received Feb. 15, 2005; revised manuscript received Jul. 8, 2005; accepted for publication Jul. 15, 2005; published online Dec. 27, 2005.

1 Introduction

Optical technologies promise high-resolution, noninvasive functional imaging of tissue with improved sensitivity, specificity, and cost effectiveness relative to current approaches. Numerous studies over the past decade have shown the viability of scattering-based optical approaches, including spectroscopy,[1–3] confocal microscopy,[4–6] and optical coherence tomography[7–9] (OCT) in addressing some of the limitations associated with current methods of cancer detection and have generated promise in differentiating normal from diseased tissue. Confocal microscopy is a rapidly developing optical technology that can noninvasively image several hundred micrometers into tissue with micrometer resolution,[10] and the capability to detect subcellular morphological changes that are potentially useful for monitoring epithelial precancers.[6] OCT is another optical method that can provide both real-time and *in situ* imaging without the necessity for removal and processing of biological samples for biopsies and histopathological assessment. The images captured are 10 to 100 times finer in detail compared to conventional imaging techniques such as magnetic resonance imaging and ultrasound and axial resolutions as fine as 1 to 2 μm have been recently demonstrated.[11] Optical coherence microscopy (OCM) is another scattering-based optical method that combines the advantages of both confocal and OCT imaging, demonstrating significant promise for epithelial cancer detection.[12] Subcellular changes that alter scattering signals, such as increased nuclear size and change in refractive index, are useful indicators of dysplasia.[13] However, many other valuable molecular indicators of early precancers may not generate obvious intrinsic optical contrast. In these cases, targeted contrast agents are desirable.

As optical imaging is still an emerging field in medical diagnostics, the application of optical contrast agents to enhance contrast of the signatures of disease is not routine. Chemical agents such as dilute acetic acid,[10,14] toluidine blue,[15,16] and Lugol's iodine[17,18] have been shown to enhance visualization of dysplasia by augmenting the overall optical properties of dysplastic tissue relative to normal surrounding tissue.[19] Acetic acid causes selective whitening of tissue and it is suggested that it alters the refractive index of the cell nucleus, causing an increased scattering effect. This effect is

Address all correspondence to Rebekah A. Drezek, Rice University, Department of Bioengineering, PO Box 1892–MS 142, Houston, Texas 77251. Tel.: 713–348–3011; Fax: 713–348–5877; E-mail: drezek@rice.edu

1083-3668/2005/10(6)/064035/10/$22.00 © 2005 SPIE

more pronounced in dysplastic regions with greater nuclear size and density. Toluidine blue is a dye that stains acidic components of cells such as the DNA and RNA. The higher level of nucleic acids present in enlarged nuclei of dysplastic cells enables the dye to enhance differentiation between normal and abnormal tissue. Lugol's iodine reacts with glycogen, present in normal epithelial tissue, while dysplastic cells and carcinomas remain comparatively unstained or lightly stained, as they contain very little tissue glycogen. Other contrast agents such as indocyanine green have been widely investigated for use in enhancing imaging and detection of cancers via fluorescence.[20,21] The dye has excitation and emission peaks near 780 and 830 nm, respectively, and this spectral region lies within the "water window" of the near IR (NIR), where photon absorption in biological tissue is at a minimum. This is most useful for detecting cancers in optical applications such as diffuse optical tomography.[22] Particle-based technologies have also generated much interest for use to enhance contrast for optical imaging and microscopy due to its optical capabilities and ease of adding surface modifications. Lee et al.[23] developed oil-filled encapsulating protein microspheres that can incorporate various particles such as gold and carbon to alter backscattering optical signatures for OCT. This can be used as a contrast agent and the enhancement was demonstrated by imaging a mouse liver with intravenously injected gold-shelled microspheres. Similarly, the use of intravenously injected polystyrene microspheres was shown to enhance imaging of skin and microcirculation under confocal reflectance microscopy.[24]

To achieve more precise and accurate diagnosis and detection of cancer, it is desirable for optical contrast agents that can target molecule specific signatures of interest. Specific targeting by therapeutic and diagnostic agents through antibody binding of tumor cell surface molecules or tumor-specific peptides has been used extensively. For example, a commercial product for the detection of prostate cancer (ProstaScint) is an antibody conjugated against prostate-specific membrane antigen also conjugated to a scintigraphic target.[25] It is also possible to achieve similar targeting efficiencies with small tumor-specific peptides.[26,27] Nanoengineered technologies and molecular targeting strategies provide an exciting nexus for further development in detection, monitoring, and biosensing of biomolecules. Technologies such as nanoprobes can be used for optical sensing of biomolecular activity in single cells, while preserving vital cellular processes.[28,29] Surfaces of nanoparticles are easily modified with antibodies, peptides, and other cell-specific moieties and can be used for applications such as glucose sensing[30] and immunoassays.[31,32] Hirsch et al. devised a simple and rapid immunoassay by successfully measuring spectral changes using gold nanoshells to target very small quantities of analytes.[31] Nanoparticles have also generated considerable interest for use as a target-specific contrast agent to enhance optical detection, diagnosis, and therapy of cancers.[33] Recent work by Sokolov et al.[34] demonstrated that the detection of precancerous cells using confocal reflectance imaging can be enhanced with gold nanoparticles bioconjugated with molecule-specific markers bound to their targets. Other nanoparticles, such as semiconductor quantum dots, also show similar potential for use as target-specific biological probes.[35,36] Quantum dots, such as ZnS-capped CdSe, are emissive at wavelengths ranging from the near-UV to the NIR by changing the size and composition. Their surfaces are also highly modifiable for bioconjugation of target-specific peptides, and it has been shown that it is possible to use such nanoparticles to bind to specific targets *in vivo* using a tumor rat model, enhancing visualization under fluorescence or confocal microscopy.[35]

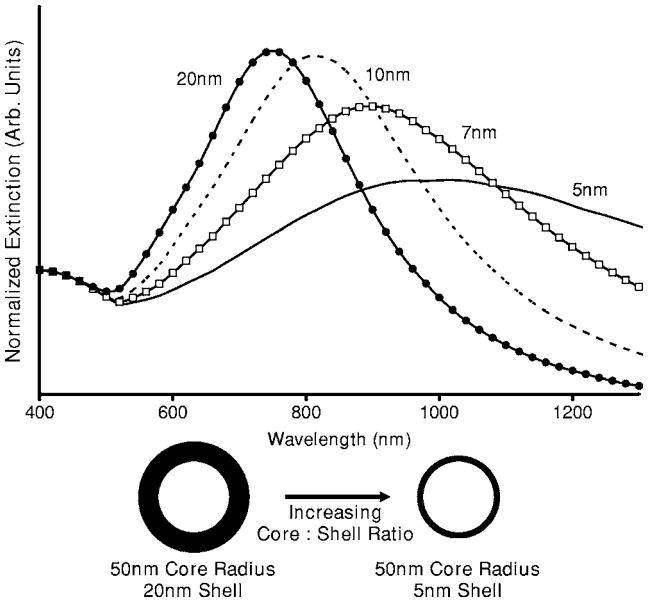

Fig. 1 By increasing the core radius to shell thickness ratio, the peak extinction resonance can be shifted well into the NIR. For gold nanoshells with a core (silica) radius of 50 nm and a decreasing gold shell thickness, the peak resonance shifts to longer wavelengths.

In this paper, we consider the use of metal nanoshells as exogenous contrast agents. Metal nanoshells are composed of a dielectric core (e.g., silica) coated with an ultrathin metallic layer (e.g., gold). Gold nanoshells possess physical properties similar to gold colloid and exhibit strong scattering and absorption effects due to the strong plasmon resonance of the metallic-dielectric concentric spherical configuration.[37,38] In particular, the optical behavior of gold nanoshells in the NIR shows scattering and/or absorption cross sections often several times the particle geometric cross section. This is not seen with comparable nanoparticles such as gold colloidal nanoparticles, which show weak optical activity in the NIR spectrum region.[38,39] By varying the relative core size and shell thickness, the peak resonance of gold nanoshells can be dramatically varied across a broad range of the optical spectrum that spans the visible and the NIR spectral regions.[40] The "tunability" of the optical resonance is a property unique to metal nanoshells. Figure 1 shows Mie extinctions plots with a 50-nm-radius silica core. By increasing the core radius-shell thickness ratio, it is possible to shift the peak plasmon resonance of the nanoshell well into the NIR and to wavelengths greater than 2 μm. Furthermore, gold nanoshells can also be tuned to show the same peak optical resonance with different size parameters.[41] Under current laboratory methods, it is also possible to fabricate gold nanoshells of varying sizes with experimental observations of gold nanoshell resonances closely matching Mie theory. The fabrication method uses a combination of molecular self-assembly and colloid chemistry

in aqueous solution and is well described in literature.[31,37]

The large optical efficiencies of nanoshells in the NIR are especially useful for biological applications. Moreover, gold nanoshells can be used for bioconjugating applications as their surfaces are virtually chemically identical to gold colloid, universally used in numerous bioconjugate applications.[42] By using nonbioconjugated gold nanoshells, Hirsch et al.[43] and O'Neal et al.[44] showed that gold nanoshells can be used as an agent for photothermal therapy of cancers. By further functionalizing gold nanoshell surfaces with target-specific antibodies, Loo et al. showed enhanced visualization using gold nanoshells targeted to HER2-positive breast cancer cells under brightfield and darkfield microscopy.[45] The targeted cancer cells can subsequently be selectively destroyed through photothermal therapy,[46] paving way for an integrated imaging and therapy of cancer. Although gold nanoshells have already shown success for cancer imaging and therapy, the optical effect of adding nanoshells to tissue has not yet been elucidated. It is important to predict how gold nanoshells affect tissue reflectance for scattering-based optical methods, so that optimal parameters for its use as an optical contrast agent can be fully realized. We evaluate gold nanoshells as an optical contrast agent with computational tools. We first use analytical electromagnetic methods to calculate optical properties of various nanoshells with a wide variety of scattering and absorbing capabilities. As the optical response of nanoshells are typically described by the optical extinction,[37,38,40] it is critical for our studies to consider the optical effect of scattering and absorption. We then employ the use of Monte Carlo methods to evaluate the effect of adding varying concentrations of gold nanoshells in tissue on photon reflectance. We also consider how the combination of scattering and absorption properties of nanoshells with different size parameters affect remitted signals. In our work, the Monte Carlo models suggest that even as the optical extinction is strongly dominated by scattering, absorption from the nanoshells cannot be neglected in predicting tissue reflectance. Furthermore, because of the strong optical behavior of nanoshells, a considerable change in reflectance was observed with only a very small concentration of nanoshells.

2 Methods

2.1 *Optical Properties of Gold Nanoshells*

The optical response of gold nanoshells can be described by using computed solutions of Mie theory for concentric spherical shells at the boundaries between different mediums.[38] For use in the Monte Carlo studies described later, Mie solutions of gold nanoshells were computed with an excitation wavelength of 830 nm, within the region of optimal physiological transmissivity best suited for optical bioimaging and biosensing applications. Typically, optical resonances of gold nanoshells are calculated with air ($n=1.0$) or water ($n=1.33$) as the embedding medium.[37,40] However, it is important that the optical properties of gold nanoshells are calculated with $n=1.4$, simulating the embedding medium as a physiological environment, as the Monte Carlo studies will use tissue models embedded with nanoshells. Table 1 shows the optical properties of the R75/115 nanoshell with $n=1.0$, 1.33, and 1.4. The differences in optical properties must be taken into account as it would subsequently affect the optical properties calculated and used in the Monte Carlo studies.

Table 1 Optical properties calculated from Mie solutions of various particles at a 830-nm excitation wavelength.

Particle	Extinction Eff.	Sca/Abs Ratio	Sca XS/Vol	Abs XS/Vol
R10-Au	0.00511	0.122	4.18×10^{4}	3.41×10^{5}
R40/45	1.614	0.059	1.50×10^{6}	2.54×10^{7}
R50/60	4.047	0.380	1.39×10^{7}	3.67×10^{7}
R40/55	2.620	0.701	1.47×10^{7}	2.10×10^{7}
R55/80	4.414	3.199	3.15×10^{7}	9.85×10^{6}
R40/80	3.738	6.270	3.02×10^{7}	4.82×10^{6}
R75/115	3.700	8.980	2.17×10^{7}	2.42×10^{6}
R75/115*	3.82	9.23	2.25×10^{7}	2.43×10^{6}
R75/115#	2.97	8.25	1.73×10^{7}	2.09×10^{6}

R40/45 represents a nanoshell with a 40-nm core radius with a 5-nm-thick gold shell. Extinction efficiencies, scattering-to-absorption efficiency ratio (Sca/Abs ratio), and the volume-normalized scattering and absorption cross sections are shown. The units for the volume-normalized cross-sections are inverse meters. Properties of the 10-nm-radius gold nanoparticle (R10-Au), a commonly used agent for biological interrogation, are included for comparison. The values shown are calculated with an embedding medium index of refraction, $n=1.4$, simulating a physiological medium. Also shown as an example, are optical property values of the R75/115 nanoshell in water (*) and air (#) with index of refraction, $n=1.33$ and $n=1.0$, respectively. The differences in the values show the importance of using the medium that more accurately mimics physiological conditions.

To choose different nanoshells with varying optical properties, we first assume independent scattering of the nanoshell particles for simplification. Under independent scattering, the optical cross section per unit volume of the particle becomes more appropriate than the optical efficiency for subsequent calculations of scattering and absorption coefficients[47,48] for use in the Monte Carlo studies. Core radius-to-shell thickness space-maps [see Figs. 2(a) and 2(b)] of volume-normalized optical cross sections are used to select the nanoshells, with a range of sizes and optical properties. The space-maps were computed with an excitation wavelength of 830 nm, including sizes that can be fabricated with current laboratory methods. As gold nanoshells possess not just scattering, but also absorbing properties, nanoshells with a variety different scattering and absorbing proportions are also considered for the Monte Carlo studies. A simple relation—the scattering-to-absorption efficiency ratio (Sca/Abs ratio)—can be used to compare how much more scattering a nanoshell is compared to its absorption ability [see Fig. 2(c)].

2.2 *Monte Carlo Modeling*

Monte Carlo modeling of photon transport in multilayered tissues by Wang et al.,[49] a computational tool written in Standard C, has been widely used to simulate random walk of photons through turbid media and is useful for investigating light propagation in tissue. The fraction of remitted and absorbed photons can be predicted from Monte Carlo computations, and the fraction changes accordingly as the optical pa-

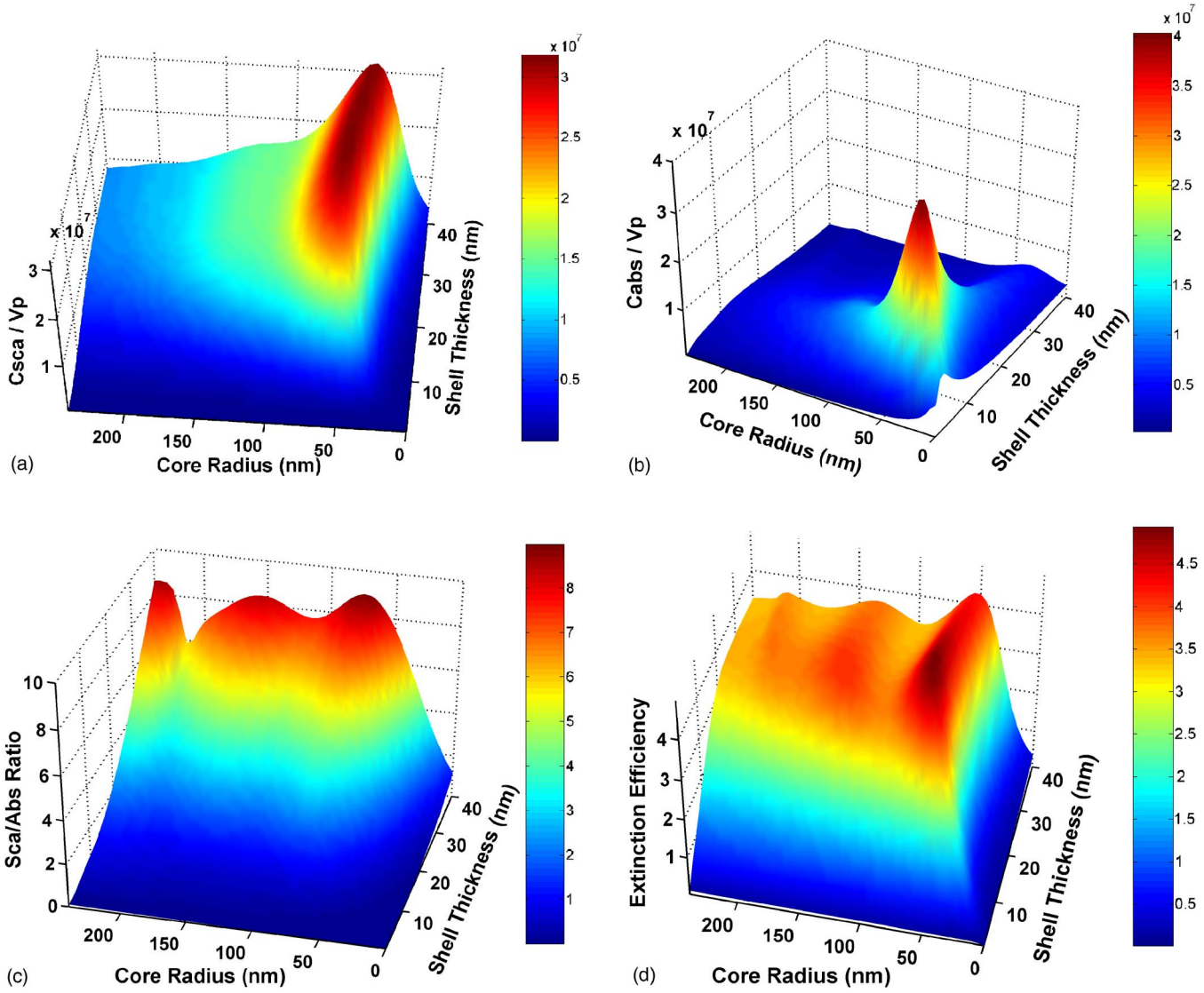

Fig. 2 Computed optical properties of gold nanoshells as a function of the core radius and the shell thickness (both in nanometers) at an excitation wavelength of 830 nm. These diagrams can aid in selecting specific nanoshells with desired optical properties. The graphs describe (a) volume-normalized scattering cross section (C_{sca}/V_p), (b) volume-normalized absorption cross section (C_{abs}/V_p), (c) scattering-to-absorption efficiency ratio (Sca/Abs), and (d) extinction efficiency. These space-maps can aid in determining the desired size and optical properties to be used in subsequent studies.

rameters of the medium are changed. The theories behind Monte Carlo methods are well described in literature and are not be repeated here.[49] Simulations were performed on two models (A and B) that will each be differentiated into two sets: a bulk tissue model (models A-1 and A-2) and a multi-layered tissue model (models B-1 and B-2). The description of the two sets is provided later. The bulk tissue model was assumed to be an infinitely thick precancerous tissue layer with uniform homogeneous optical properties. The base optical properties before the addition of nanoshells of this precancerous layer was set with the absorption coefficient at $\mu_{abs(c)}=0.05\ cm^{-1}$, and the scattering coefficient, $\mu_{sca(c)}=50\ cm^{-1}$, both within cited literature[50–52] values in the NIR. The tissue properties of this layer are then changed, simulating an increasing concentration of nanoparticles added to the tissue.

A three-layered model (models B-1 and B-2) used in our studies (see Fig. 3) is similar to the theoretical model used by Quan and Ramanujam,[53] which mimics the basic structure of epithelial and stromal tissue. The first layer represents normal surface epithelium with a thickness of $d_1=175\ \mu m$, and optical parameters were kept constant at $\mu_{sca(1)}=50\ cm^{-1}$ and $\mu_{abs(1)}=1.5\ cm^{-1}$. The second precancerous layer ($d_2=175\ \mu m$), originates from the basal membrane, occupying space between the stroma and the normal epithelium of the top layer. As the epithelium consists of the most superficial tissue layers, hemoglobin content is negligible. The absorption coefficients of the epithelial layers represent absorption by tissue chromophores such as lipid, water and cytochrome oxidase.[54–56] Similar to model A, increasing concentrations of nanoshells were added to this representative precancerous

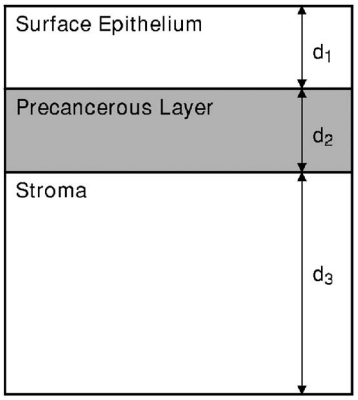

Fig. 3 Schematic showing the multilayered tissue model used in the Monte Carlo studies. The depths of the parameters shown are: normal surface epithelium, $d_1=175\ \mu$m; precancerous layer, $d_1=175\ \mu$m; and stromal layer (semi-infinitely thick), $d_3=1.0\times10^8$ cm. The optical parameters of the layers were set as, normal surface epithelium, $\mu_{sca(1)}=50\ cm^{-1}$ and $\mu_{abs(1)}=1.5\ cm^{-1}$, and the stromal layer optical properties of $\mu_{sca(3)}=250\ cm^{-1}$ and $\mu_{abs(3)}=1.5\ cm^{-1}$. The concentration of nanoparticles was incremented in the precancerous layer, with base optical properties of $\mu_{sca(c)}=50\ cm^{-1}$ and $\mu_{abs(c)}=0.05\ cm^{-1}$.

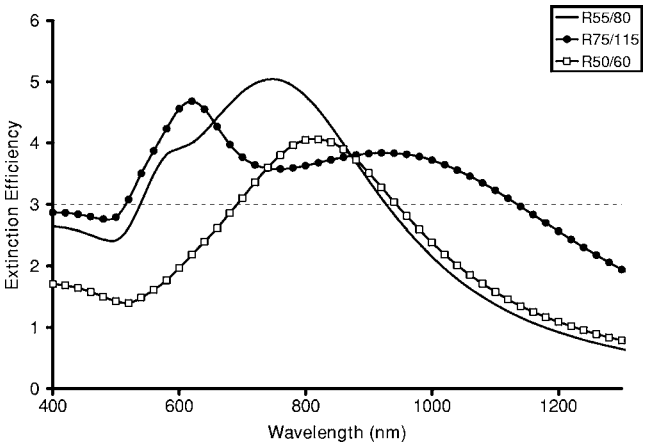

Fig. 4 Representative extinction efficiencies of three different nanoshells, R75/115, R50/60, and R55/80, used in the Monte Carlo experiments. The different extinction profiles are plotted against a broad wavelength range, showing optical activity well into the NIR. Nanoshells of different sizes produce unique and different optical responses.

layer and the optical properties of this second layer without any nanoshells was the same as the bulk tissue, where $\mu_{sca(c)}=50\ cm^{-1}$ and $\mu_{abs(c)}=0.05\ cm^{-1}$. The stromal layer was modeled as a semi-infinitely thick ($d_3=1.0\times10^8$ cm) layer with $\mu_{sca(3)}=250\ cm^{-1}$ and $\mu_{abs(3)}=1.5\ cm^{-1}$. The following properties were kept constant for all simulations: the anisotropy factor (g) was kept constant at 0.9 and $n=1.4$ for the tissue refractive index.

The overall scattering $[\mu_{sca(t)}]$ and absorption coefficient $[\mu_{abs(t)}]$ of the tissue is altered by the optical properties of the particles added to the models. As a basis of comparison, gold nanoparticles (10 nm radius) commonly used for biological interrogation such as biomolecular analysis, interactions, and imaging[34,57,58] were used in place of the gold nanoshells. To account for interparticle effects by the nanoparticles on photon scattering, a correction factor is required for volume fractions higher[59,60] than ~1%, when the diameter of the particles are much less than the wavelength to account for the reduction of bulk optical cross section as a result of nonindependent scattering among subwavelength spheres. As mentioned, for these studies, we impose a limit on the density and size of nanoshells added to the precancerous layers to ensure independent scattering. Each type of nanoparticles is then added separately, so that only one type of particle is added to the models at one time. Using well established light scattering theory, the change in the optical coefficient $[\Delta\mu_{(p)}]$ due to particles in a medium, is related to the scattering or absorption cross section (C) and the number of particles per unit volume[48] (N):

$$\Delta\mu_{(p)} = N \times C.$$

This can then be related to the volume fraction (V_f) of nanoparticles added to the models, and also the scattering (C_{sca}) or absorption cross section (C_{abs}) normalized by the volume of the particle used (V_p),

$$\Delta\mu_{sca,abs(p)} = \frac{C_{sca,abs}}{V_p} V_f.$$

The change in scattering or absorption coefficient $[\Delta\mu_{(p)}]$ can be due to the scattering or absorption of the particle added. To evaluate the overall effect adding particles with a variety of physical and optical parameters, the studies are separated into two sets for both the bulk (model A) and multilayered (model B) models. As gold nanoshells can be fabricated to be far more scattering than absorbing, for example, the R75/115 (representing a core radius of 75 nm and an overall radius of 115 nm) gold nanoshell shows almost 90% of the extinction as scattering, we access if such highly scattering particles can be simply considered as a scatterer while neglecting its absorption properties. Thus, the studies will be further separated into two sets, one considering only the scattering properties of the particles and neglecting the absorption. The other will take

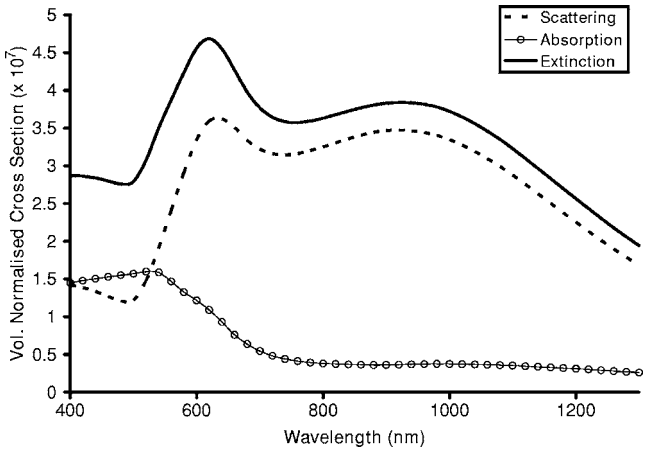

Fig. 5 Volume normalized cross sections of the R75/115 gold nanoshell ($n=1.4$). Although the scattering property of the nanoshell generally dominates the absorption, it is expected that the diffuse reflectance of tissue with nanoshells will decrease across wavelength.

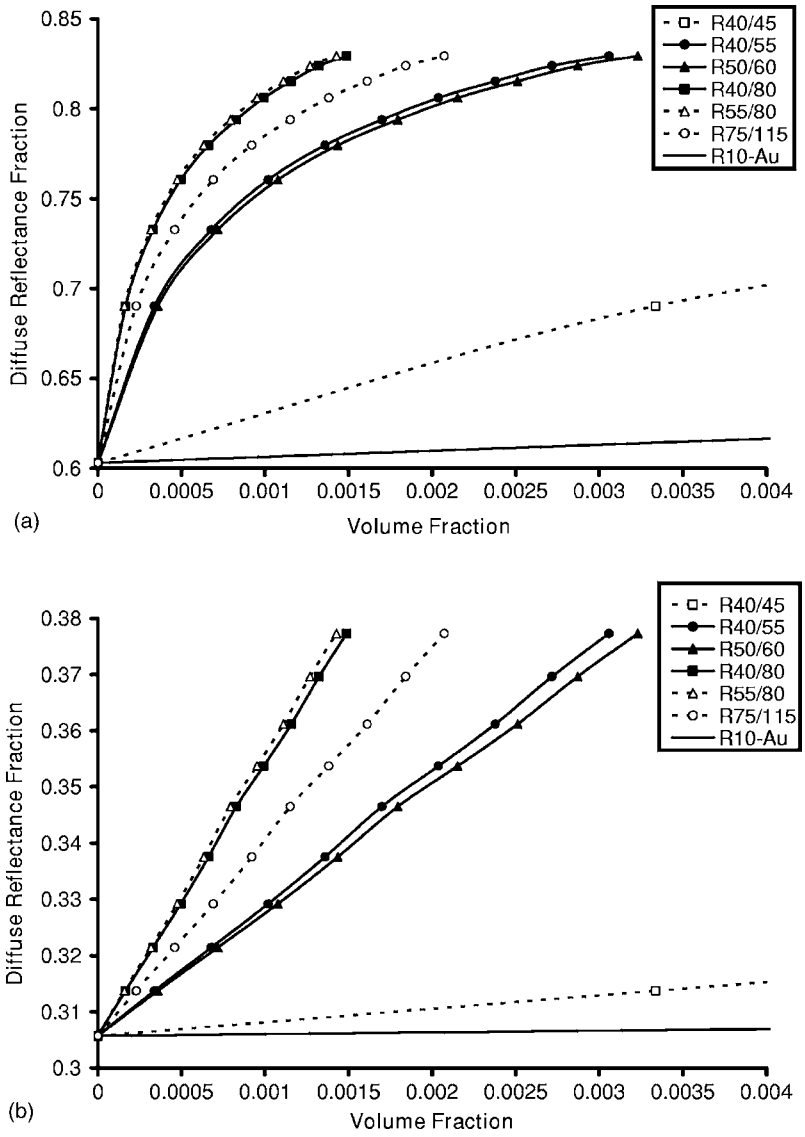

Fig. 6 Diffuse reflectance from the (a) bulk (model A-1) and (b) multilayered (model B-1) models with $\mu_{abs(c)}=0.05\ cm^{-1}$, using different types of nanoparticles. The higher the volume-normalized scattering cross section, the more the diffuse reflectance increases with the same volume fraction of nanoshells added. The results show the studies that neglected absorption from the nanoparticles, assuming the particles as simple scatterers.

into account both the scattering and absorption properties of the particles. For the first set (models A-1 and B-1), as only the scattering effect by the nanoparticles $[\Delta\mu_{sca(p)}]$ is considered for the change of the overall scattering properties of the tissue $[\mu_{sca(t)}]$, the tissue absorption therefore does not change and remains at the base level $[\mu_{abs(c)}=0.05\ cm^{-1}]$. The overall scattering $[\mu_{sca(t)}]$ and absorption coefficient $[\Delta\mu_{abs(p)}]$ of set 1 can be related through

$$\mu_{abs(t)} = \mu_{abs(c)},$$

$$\mu_{sca(t)} = \mu_{sca(c)} + \Delta\mu_{sca(p)}.$$

In the second set (models A-2 and B-2), the combination of both scattering and absorption by the nanoparticles are taken into consideration. The respective change in absorption coefficient $[\Delta\mu_{abs(p)}]$ can then also be calculated using a similar relation. Both the overall scattering $[\mu_{sca(t)}]$ and absorption coefficients $[\mu_{abs(t)}]$ of tissue are consequently altered by the optical response of the nanoshells. Thus the overall change in optical properties of the precancerous layer is,

$$\mu_{abs(t)} = \mu_{abs(c)} + \Delta\mu_{abs(p)},$$

$$\mu_{sca(t)} = \mu_{sca(c)} + \Delta\mu_{sca(p)}.$$

From this set of Monte Carlo studies, we evaluate the effect of absorption from nanoshells on tissue reflectance with absorption and/or scattering dominated gold nanoshells, and compare this to the results from set 1.

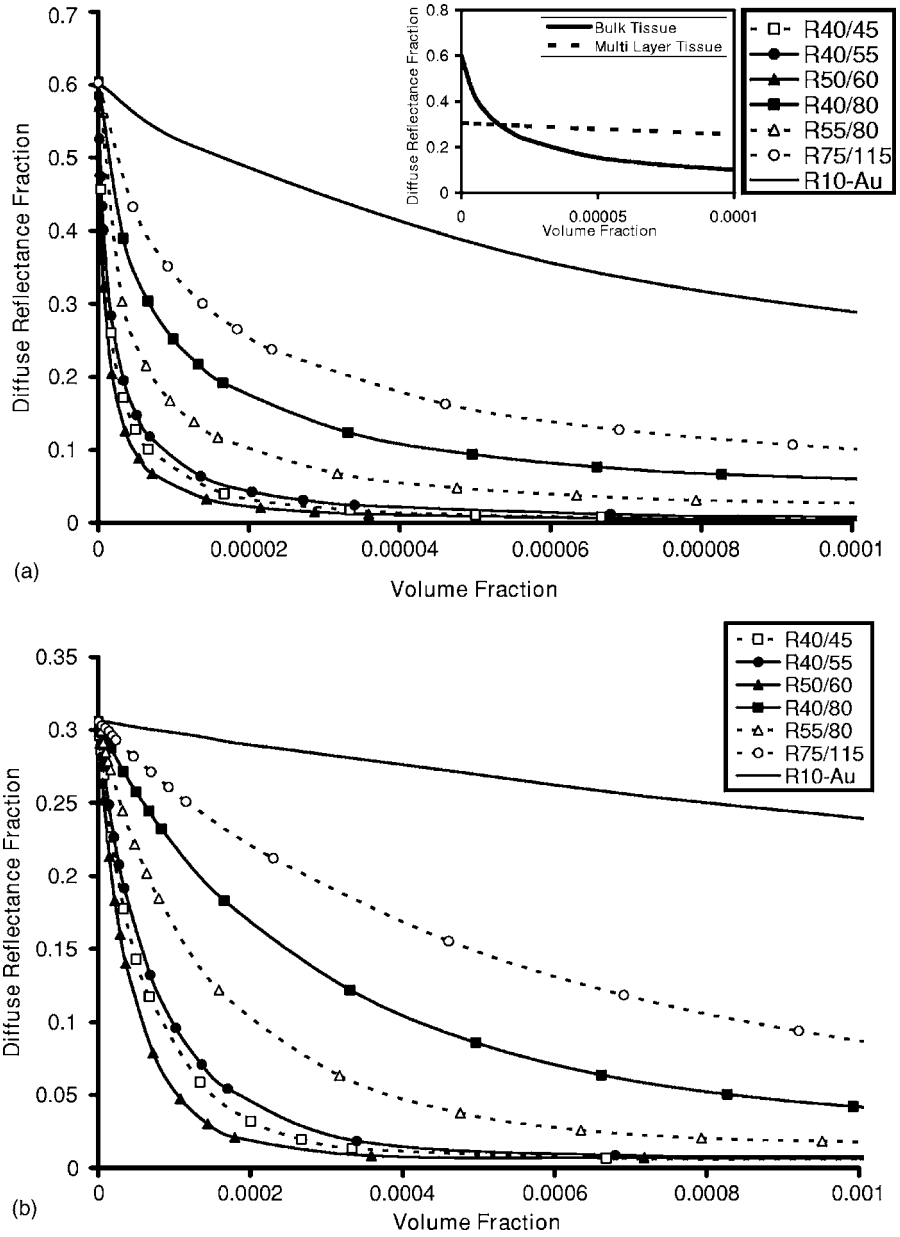

Fig. 7 Diffuse reflectance from the (a) bulk (model A-2) and (b) multilayered (model B-2) tissue when both scattering and absorption from the nanoparticles were considered. As the volume-normalized absorption cross section of the particle increases, the reflectance decreases. Model B-2 shows a more gradual decrease in reflectance compared to model A-2, and eventually shows higher reflectance as more particles were added, even though model A-2 showed higher reflectance before any nanoparticles were added. To describe this, the insert shown in (a) shows comparison of the diffuse reflectance fraction from the bulk (solid line) and multilayered (dotted line) models with increasing volume fractions of the R75/115 nanoshell.

3 Results and Discussion

3.1 *Gold Nanoshells*

Figures 2(a)–2(d) shows various optical properties of gold nanoshells compared to core radius and shell thicknesses up to an overall radius of 280 nm at an excitation wavelength of 830 nm. The figures show the volume normalized scattering cross section [Fig. 2(a)], volume normalized absorption cross section [Fig. 2(b)], and the scattering-to-absorption efficiency ratio [Fig. 2(c)]. Figure 2(d) shows the extinction efficiency of the nanoshells. Using these space-maps of optical properties, nanoshells of different sizes and properties (also see Table 1) were chosen and their effect on tissue diffuse reflectance investigated. The table shows that the particles with the highest scattering and absorption efficiencies do not necessarily show the highest optical cross sections per unit volume of the particle, and this becomes important and are described later. To further describe the optical versatility of gold nanoshells, Fig. 4 shows representative optical extinction profiles of some of the nanoshells (R75/115, R50/60, and R55/80) used in these studies showing very different responses across wavelengths. Figure 5 shows volume-normalized absorption, scattering and extinction of the R75/115 nanoshell.

3.2 *Monte Carlo Studies*

The Monte Carlo studies show that the addition of gold nanoshells to tissue causes a significant change in tissue reflectance. It is also possible to detect the change in reflectance due to a buried layer of tissue containing nanoshells. Between Monte Carlo modeling sets 1 and 2, the absorption properties of nanoshells are an important factor for predicting the tissue reflectance and cannot be neglected, even if the optical properties of the particle is dominated by scattering. The gold nanoshells were observed to scatter or absorb light far more efficiently than the gold nanoparticles. A large change in reflectance was observed with only a very small amount of nanoshells, while the gold nanoparticle caused little change in reflectance.

In set 1 of the Monte Carlo studies, the diffuse reflectance generally increased as the amount of nanoshells added increased. Figures 6(a) and 6(b) shows the diffuse reflectance results from the bulk (model A-1) and multilayered (model B-1) tissue models after gold nanoshells of a variety of scattering properties and the 10-nm gold nanoparticles were added to the tissue with increasing concentration. The reflectance increases after the addition of gold nanoshells, while the results from the gold colloid particle remain relatively unchanged. The photon reflectance, before adding any nanoparticles, is approximately 0.6 from model A-1 and 0.3 from model B-1. With the same concentration of particles added, the particle with the greater volume-normalized scattering cross sections shows higher reflectance. For example, the R55/80 nanoshell exhibits the highest reflectance, while the R40/45 shows the lowest of all the nanoshells. This corresponds to the volume-normalized scattering cross-section values as shown in Table 1. The R55/80 nanoshell exhibits the highest volume-normalized scattering cross section (Abs XS/Vol=3.15×10^{7} m^{-1}) and the R40/45 nanoshell had the lowest value among the gold nanoshells used, with Abs XS/Vol=1.50×10^{6} m^{-1}. The 10 nm radius gold colloid particle (R10-Au) with the lowest volume-normalized scattering cross section correspondingly shows very little change in both models A-1 and B-1.

In set 2, the results, when absorption from gold nanoshells and gold colloid $[\Delta\mu_{abs(p)}]$ was considered together with the scattering, are shown in Figs. 7(a) and 7(b). The results also show an immediate decrease in reflectance after the nanoparticles were included. When the concentration of the particles was increased, the diffuse reflectance decreased, and this occurred for all the particle configurations used in the simulations. Furthermore, the diffuse reflectance from model A-2 decreases more rapidly compared to model B-2 and eventually shows higher reflectance for the same amount of nanoshells added, as shown in the inset of Fig. 7(a). The graph shows that at a volume fraction of 0.00005, the reflectance with the R75/115 gold nanoshell is approximately 0.15 in model A-2, and about 0.28 from model B-2. Compared to when no particles were added to the tissue, the reflectances are approximately 0.3 (model B-2) and 0.6 (model A-2). Further increases in concentration diminish the reflectance close to zero. The uniform change in the optical properties of the bulk model (model A-2), leads to a higher probability that photons will be absorbed in the topmost regions, whereas in model B-2, as the precancerous layer is buried away from the surface, there are greater chances of scattering when the photons first travel through the surface epithelium.

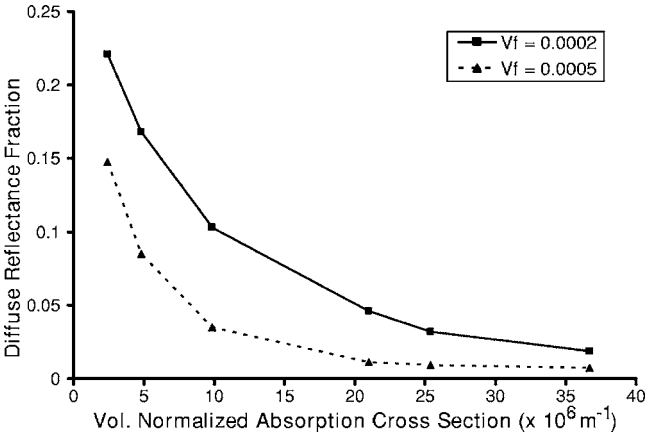

Fig. 8 The diffuse reflectance as a function of the volume normalized absorption cross section of different gold nanoshells used in the multilayered Monte Carlo studies (refer to Table 1). As the volume normalized absorption increases, the reflectance correspondingly decreases. Volume fractions (V_f) of 0.0002 and 0.0005 are shown, within the constraints for independent scattering.

Even as it is useful to use the scattering-to-absorption ratio (Abs/Sca ratio) of the optical properties to describe how much more scattering the particle is compared to absorption, the volume-normalized absorption cross section of the particles is a more adequate description of how the optical properties of the particles influences tissue reflectance in our studies. The comparison of the scattering and absorbing properties of each particle is shown in Table 1 under Abs/Sca Ratio. For example, the R75/115 nanoshell shows a scattering cross section of almost 9 times over the absorption cross section, while the scattering of the R40/45 nanoshell is about 5.9% that of its absorption. Comparing this to the reflectance, the R75/115 and R40/45 nanoshells, however, do not show the highest and lowest reflectances, respectively. Thus, we can infer that absorption from the particles has a far greater effect on reflectance and cannot be neglected, even if the particle possess scattering cross section several times larger than its absorption. When we consider only scattering from the nanoparticles in models A-1 and B-1, it is obvious that higher scattering cross section per unit volume of the particle shows higher reflectance with the limitation of independent scattering. However, with different configurations of scattering and absorption from the gold nanoshells, the reflectance is more dependent on the volume-normalized absorption cross section than the combination of scattering and absorption. Figure 8 shows the relationship between diffuse reflectance and volume-normalized absorption cross sections of gold nanoshells. The diffuse reflectance decreases correspondingly (volume fraction, V_f=0.0002 and 0.0005) as the absorption of gold nanoshells increase. This reemphasizes the importance of absorption from the particles and suggests that gold nanoshells can more efficiently lower the photon reflectance compared to gold colloid. This can be potentially useful for enhancing reflectance signatures through absorption for spectroscopic detection modalities. Furthermore, only a very small number of nanoshells are required to produce an observable

change in the remitted signal. The volume-normalized absorption cross section of the R75/115 nanoshell shown in Fig. 5 range from 1.6×10^{7} m^{-1} at 520 nm to 3.74×10^{6} m^{-1} at 1000 nm ($n=1.4$). As spectroscopic methods typically use a range of wavelengths, comparing these values to the R10-Au gold nanoparticle, these values are still considerably larger. Thus, when comparing normal tissue and nanoshell targeted tissue, the spectra of the diseased tissue would likely show a much reduced spectral intensity with the presence of nanoshells, which would provide an indication of the presence of targeted cells.

Throughout the Monte Carlo simulations, the anisotropy (g) of the tissue was assumed to remain constant with the addition of the particles. From Mie solutions of the gold nanoshells, the g values for the nanoshells can be calculated, and the overall effect on the anisotropy of the tissue is related by,

$$g_{\text{overall}} = (g_{\text{tissue}})(1 - V_f) + (g_{\text{nanoshell}})(V_f),$$

where V_f is the volume fraction of the nanoshells as described before, and $1-V_f$ is the volume fraction of the tissue not occupied by the nanoshells. With such a low-volume fraction of nanoshells, the overall change in the anisotropy of the tissue is very small and can be assumed as negligible. For instance, the R40/80 nanoshell has a g value of approximately -0.033 at an excitation wavelength of 830 nm in physiological media ($n=1.4$). At a volume fraction of $V_f=0.0005$, the change in the g value of the tissue ($g=0.9$) is less than 0.0005, not enough to significantly alter the reflectance.

4 Conclusions

Gold nanoshells possess unique and tunable optical signatures, in particular, strong optical responses in the NIR, desirable for biological applications. Gold nanoshells are easily fabricated for size and desired optical response under current chemistries. The absorption of gold nanoshells is critical in predicting the macroscopic behavior of light transport through turbid media embedded with nanoshells. The large scattering cross section of gold nanoshells in the NIR has already been exploited and demonstrated[61] to enhance contrast for imaging in OCT. In addition, the strong absorption capabilities has been used in new imaging technologies such as photoacoustic tomography on the rat brain *in vivo*,[62] further underlining the cross-platform potential of gold nanoshells for integrated imaging, diagnosis, and therapy of cancers. By exploring gold nanoshells with different physical parameters, we can continue to investigate the effects of changing nanoshell properties, possibly optimizing nanoshells with parameters best suited for different imaging and spectroscopic modalities. The studies reported in this paper strongly suggest that the strong optical responses of gold nanoshells can be utilized to alter signatures for scattering-based optical diagnostic methods.

Acknowledgments

We would like to acknowledge Joe Jackson and Lee Hirsch for their invaluable advice and help on the Mie computations and gold nanoshell fabrication. Funding for this project was provided by the National Science Foundation (BES 022-1544), the National Science Foundation Center for Biological and Environmental Nanotechnology (EEC-0118007), and the Department of Defense Congressionally Directed Medical Research Program (DAMD17-03-1-0384).

References

1. H. Zeng, M. Petek, M. T. Zorman, A. McWilliams, B. Palcic, and S. Lam, "Integrated endoscopy system for simultaneous imaging and spectroscopy for early lung cancer detection," *Opt. Lett.* **29**(6), 587–589 (2004).
2. A. Amelink, H. J. C. M. Sterenborg, M. P. L. Bard, and S. A. Burgers, "*In vivo* measurement of the local optical properties of tissue by use of differential path-length spectroscopy," *Opt. Lett.* **29**(10), 1087–1089 (2004).
3. K. Sokolov, L. T. Nieman, A. Myakov, and A. Gillenwater, "Polarized reflectance spectroscopy for pre-cancer detection," *Technol. Cancer Res. Treat.* **3**(1), 1–14 (2004).
4. C. Liang, K. B. Sung, R. R. Richards-Kortum, and M. R. Descour, "Design of a high-numerical-aperture miniature microscope objective for an endoscopic fiber confocal reflectance microscope," *Appl. Opt.* **41**(22), 4603–4610 (2002).
5. K. B. Sung, C. Liang, M. Descour, T. Collier, M. Follen, and R. Richards-Kortum, "Fiber-optic confocal reflectance microscope with miniature objective for *in vivo* imaging of human tissue," *IEEE Trans. Biomed. Eng.* **49**(10), 1168–1172 (2002).
6. T. Collier, A. Lacy, R. Richards-Kortum, A. Malpica, and M. Follen, "Near real-time confocal microscopy of amelanotic tissue," *Acad. Radiol.* **9**(5), 504–512 (2002).
7. T. Q. Xie, M. L. Zeidel, and Y. T. Pan, "Detection of tumorigenesis in urinary bladder with optical coherence tomography: optical characterization of morphological changes," *Opt. Express* **10**, 1431–1443 (2002).
8. J. G. Fujimoto, "Optical coherence tomography for ultrahigh resolution *in vivo* imaging," *Nat. Biotechnol.* **21**(11), 1361–1367 (2003).
9. E. S. Matheny, N. M. Hanna, W. G. Jung, Z. Chen, P. Wilder-Simth, R. Mina-Araghi, and M. Brenner, "Optical Coherence Tomography of malignancy in hamster cheek pouces," *J. Biomed. Opt.* **9**(5), 978–981 (2004).
10. R. A. Drezek, T. Collier, C. K. Brookner, A. Malpica, R. Lotan, R. R. Richards-Kortum, and M. Follen, "Laser scanning confocal microscopy of cervical tissue before and after application of acetic acid," *Am. J. Obstet. Gynecol.* **182**, 1135–1139 (2000).
11. W. Drexler, U. Morgner, F. X. Kartner, C. Pitris, S. A. Boppart, X. D. Li, E. P. Ippen, and J. G. Fujimoto, "*In vivo* ultrahigh resolution optical coherence tomography," *Opt. Lett.* **24**, 1221–1223 (1999).
12. A. L. Clark, A. Gillenwater, R. Alizadeh-Naderi, A. K. El-Naggar, and R. Richards-Kortum, "Detection and diagnosis of oral neoplasia with an optical coherence microscope," *J. Biomed. Opt.* **9**(6), 1271–1280 (2004).
13. R. Drezek, T. Collier, C. MacAulay, M. Follen, and R. Richards-Kortum, "Light scattering from cervical cells throughout neoplastic progression: influence of nuclear size, DNA content, and chromatin texture," *J. Biomed. Opt.* **8**, 7–16 (2003).
14. T. Collier, P. Shen, B. de Pradier, K. B. Sung, R. Richards-Kortum, A. Malpica, and M. Follen, "Near real time confocal microscopy of amelanotic tissue: dynamics of aceto-whitening enable nuclear segmentation," *Opt. Express* **6**(2), 40–48 (2000).
15. M. A. Onofre, M. R. Sposto, and C. M. Navarro, "Reliability of toluidine blue application in the detection of oral epithelial dysplasia and in situ and invasive squamous cell carcinomas," *Oral Surg. Oral Med. Oral Pathol. Oral Radiol. Endod.* **91**(5), 535–540 (2001).
16. I. C. Martin, C. J. Kerawala, and M. Reed, "The application of toluidine blue as a diagnostic adjunct in the detection of epithelial dysplasiam," *Oral Surg. Oral Med. Oral Pathol. Oral Radiol. Endod.* **85**(4), 444–446 (1998).
17. A. J. Tincani, N. Brandalise, A. Altemani, R. C. Scanavini, J. B. M. Valerio, H. T. Lage, G. Molina, and A. S. Martins, "Diagnosis of superficial esophageal cancer and dysplasia using endoscopic screening with a 2% Lugol dye solution in patients with head and neck cancer," *Head Neck* **22**(2), 170–174 (2000).
18. Y. Nakanishi, A. Ochiai, K. Yoshimura, H. Kato, T. Shimoda, H. Yamaguchi, Y. Tachimori, H. Watanabe, and S. Hirohashi, "The clinicopathologic significance of small areas unstained by Lugol's iodine in the mucosa surrounding resected esophageal carcinoma," *Cancer* **82**(8), 1454–1459 (1998).

19. A. F. Zuluaga, R. Drezek, T. Collier, R. Lotan, M. Follen, and R. Richards-Kortum, "Contrast agents for confocal images of normal and cancer cells in suspension," *J. Biomed. Opt.* **7**(3), 398–403 (2002).
20. E. M. Sevick-Muraca, J. P. Houston, and M. Gurfinkel, "Fluorescence-enhanced, near infrared diagnostic imaging with contrast agents," *Curr. Opin. Chem. Biol.* **6**, 642–650 (2002).
21. A. Godavarty, A. B. Thompson, R. Roy, M. Gurfinkel, M. J. Eppstein, C. Zhang, and E. M. Sevick-Muraca, "Diagnostic imaging of breast cancer using fluorescence-enhanced optical tomography," *J. Biomed. Opt.* **9**(3), 488–496 (2004).
22. V. Ntziachristos, A. G. Todh, M. Schnall, and B. Chance, "Concurrent MRI and diffuse optical tomography of breast after indocyanine green enhancement," *Proc. Natl. Acad. Sci. U.S.A.* **97**(6), 2767–2772 (2000).
23. T. M. Lee, F. J. Toublan, S. Sitafalwalla, A. L. Oldenburg, K. S. Suslick, and S. A. Boppart, "Engineered microsphere contrast agents for optical coherence tomography," *Opt. Lett.* **28**(17), 1546–1548 (2003).
24. M. Rajadhyaksha, S. Gonzalez, and J. M. Zavislan, "Detectability of contrast agents for confocal reflectance imaging of skin and microcirculation," *J. Biomed. Opt.* **9**(2), 323–331 (2004).
25. A. K. Gregorakis, E. H. Holmes, and G. P. Murphy, "Prostate-specific membrane antigen: current and future utility," *Semin Urol. Oncol.* **16**(1), 2–12 (1998).
26. M. Kolonin, R. Pasqualini, and W. Arap, "Molecular addresses in blood vessels as targets for therapy," *Curr. Opin. Chem. Biol.* **5**(3), 308–313 (2001).
27. U. Mahmood, C. H. Tung, A. Bogdanov, Jr., and R. Weissleder, "Near-infrared optical imaging of protease activity for tumor detection," *Radiology* **213**(3), 866–870 (1999).
28. P. M. Kasili, J. M. Song, and T. Vo-Dinh, "Optical sensor for the detection of caspase-9 activity in a single cell," *J. Am. Chem. Soc.* **126**(9), 2799–2806 (2004).
29. J. M. Song, P. M. Kasili, and T. Vo-Dinh, "Detection of cytochrome *c* in a single cell using and optical nanobiosensor," *Anal. Chem.* **76**(9), 2591–2594 (2004).
30. K. Aslan, J. R. Lackowicz, and C. D. Geddes, "Nanogold-plasmon-resonance-based glucose sensing," *Anal. Biochem.* **330**(1), 145–155 (2004).
31. L. R. Hirsch, J. B. Jackson, A. Lee, N. J. Halas, and J. L. West, "A whole blood immunoassay using gold nanoshells," *Anal. Chem.* **75**, 2377–2381 (2003).
32. J. R. Lakowicz, J. Malicka, J. Huang, Z. Gryczynski, and I. Gryczynski, "Ultrabright fluorescein-labeled antibodies near silver metallic surfaces," *Biopolymers* **74**, 467–475 (2004).
33. I. Brigger, C. Dubernet, and P. Couvreur, "Nanoparticles in cancer therapy and diagnosis," *Adv. Drug Delivery Rev.* **54**, 631–651 (2002).
34. K. Sokolov, M. Follen, J. Aaron, I. Pavlova, A. Malpica, R. Lotan, and R. Richards-Kortum, "Real-time vital optical imaging of precancer using anti-epidermal growth factor receptor antibodies conjugated to gold nanoparticles," *Cancer Res.* **63**, 1999–2004 (2003).
35. M. E. Akerman, W. C. W. Chan, P. Laakkonen, S. N. Bhatia, and E. Ruoslahti, "Nanocrystal targeting *in vivo*," *Proc. Natl. Acad. Sci. U.S.A.* **99**(20), 12617–12621 (2002).
36. W. C. W. Chan, D. J. Maxwell, X. Gao, R. E. Bailey, M. Y. Han, and S. Nie, "Luminescent quantum dots for multiplexed biological detection and imaging," *Curr. Opin. Biotechnol.* **13**, 40–46 (2002).
37. S. J. Oldenburg, R. D. Averitt, S. L. Westcott, and N. J. Halas, "Nanoengineering of optical resonance," *Chem. Phys. Lett.* **288**, 243–247 (1998).
38. R. D. Averitt, S. L. Westcott, and N. J. Halas, "Linear optical properties of gold nanoshells," *J. Opt. Soc. Am. B* **16**(10), 1824–1832 (1999).
39. U. Kreibig and M. Vollmer, *Optical Properties of Metal Clusters*, Springer-Verlag, Berlin (1995).
40. S. J. Oldenburg, J. B. Jackson, S. L. Westcott, and N. J. Halas, "Infrared extinction properties of gold nanoshells," *Appl. Phys. Lett.* **75**(19), 2897–2899 (1999).
41. C. Loo, A. Lin, L. Hirsch, M. Lee, J. Barton, N. Halas, J. West, and R. Drezek, "Nanoshell-enabled photonics-based imaging and therapy of cancer," *Technol. Cancer Res. Treat.* **3**(1), 33–40 (2004).
42. W. T. Faulk and G. Taylor, "An immunocolloid method for the electron microscope," *Immunochemistry* **8**(11), 1081–1083 (1971).
43. L. R. Hirsch, R. J. Stafford, J. A. Bankson, S. R. Sershen, B. Rivera, R. E. Price, J. D. Hazle, N. J. Halas, and J. L. West, "Nanoshell-mediated near-infrared thermal therapy of tumors under magnetic resonance guidance," *Proc. Natl. Acad. Sci. U.S.A.* **23**, 13549–13554 (2003).
44. D. P. O'Neal, L. R. Hirsch, N. J. Halas, J. D. Payne, J. L. West, "Photo-thermal tumor ablation in mice using near infrared-absorbing nanoparticles," *Cancer Lett.* **109**, 181–176 (2004).
45. C. Loo, L. Hirsch, M. Lee, E. Chang, J. West, N. Halas, and R. Drezek, "Gold nanoshell bioconjugates for molecular imaging in living cells," *Opt. Lett.* **30**(9), 1012–1014 (2004).
46. C. Loo, A. Lowery, N. Halas, J. West, and R. Drezek, "Immunotargeted nanoshells for integrated cancer imaging and therapy," *Nano Lett.* **5**(4), 709–711 (2005).
47. G. Zaccanti, S. Del Bianco, and F. Martelli, "Measurements of optical properties of high-density media," *Appl. Opt.* **42**(19), 4023–4030 (2003).
48. H. C. van der Hulst, *Light Scattering by Small Particles*, Dover Press, New York (1981).
49. L. H. Wang, S. L. Jacques, and L. Q. Zheng, "MCML—Monte Carlo modeling of photon transport in multi-layered tissues," *Comput. Methods Programs Biomed.* **47**, 131–146 (1995).
50. R. Hornung, T. H. Pham, K. A. Keefe, M. W. Berns, Y. Tadir, and B. J. Tromberg, "Quantitative near-infrared spectroscopy of cervical dysplasia *in vivo*," *Hum. Reprod.* **14**(11), 2908–2916 (1999).
51. A. Toricelli, A. Pifferi, P. Taroni, E. Giambattistelli, and R. Cubeddu, "*In vivo* optical characterization of human tissues from 610–1010 nm by time-resolved reflectance spectroscopy," *Phys. Med. Biol.* **46**, 2227–2237 (2001).
52. R. M. P. Doornbos, R. Lang, M. C. Aalders, F. W. Cross, and H. J. C. M. Sterenborg, "The determination of *in vivo* human tissue optical properties and absolute chromophore concentrations using spatially resolved steady-state diffuse reflectance spectroscopy," *Phys. Med. Biol.* **44**, 967–981 (1999).
53. L. Quan and N. Ramanujam, "Relationship between depth of a target in a turbid medium and fluorescence measured by a variable-aperture method," *Opt. Lett.* **27**(2), 104–106 (2002).
54. R. L. P. van Veen, H. J. C. M. Sterenborg, A. Pifferi, A. Torricelli, and R. Cubeddu, "Determination of VIS-NIR absorption coefficients of mammalian fat, with time- and spatially resolved diffuse reflectance and transmission spectroscopy," in *Proc. Biomedical Topical Meetings*, on CD-ROM, Paper SF5, Optical Society of America, Washington, DC (2004).
55. A. Akin, "Functional imaging using near infrared light," in *Proc. of ISIK2000 Workshop on Biomedical Information Engineering*, pp. 209–212, Istanbul, Turkey (2000).
56. B. Chance, M. Cope, E. Gratton, N. Ramanujam, and B. Tromberg, "Phase measurement of light absorption and scatter in human tissue," *Rev. Sci. Instrum.* **69**(10), 3457–3481 (1998).
57. N. T. K. Thanh and Z. Rosenberg, "Development of an aggregation-based immunoassay for anti-protein A using gold nanoparticles," *Anal. Chem.* **74**, 1624–1628 (2002).
58. C. H. Teng, K. C. Ho, Y. S. Lin, and Y. C. Chen, "Gold nanoparticles as selective and concentrating probes for samples in MALDI MS analysis," *Anal. Chem.* **76**, 4337–4342 (2004).
59. A. Ishimaru and Y. Kuga, "Attenuation constant of a coherent field in a dense distribution of particles," *J. Opt. Soc. Am.* **72**, 1317–1320 (1982).
60. J. M. Schmitt and G. Kumar, "Optical scattering properties of soft tissue: a discrete particle model," *Appl. Opt.* **37**(3), 2788–2797 (1998).
61. J. K. Barton, N. J. Halas, J. L. West, and R. A. Drezek, "Nanoshells as an optical coherence tomography contrast agent," *Proc. SPIE* **5316**, 99–106 (2004).
62. Y. Wang, X. Xie, X. Wang, G. Ku, K. L. Gill, D. P. O'Neal, G. Stoica, and L. V. Wang, "Photoacoustic tomography of a nanoshell contrast agent in the in vivo rat brain," *Nano Lett.* **4**(9), 1689–1692 (2004).